

MoS₂: a Choice Substrate for Accessing and Tuning the Electronic Properties of Graphene

Chih-Pin Lu^{1,2}, Guohong Li¹, K. Watanabe³, T. Taniguchi³ and Eva Y. Andrei¹

¹*Department of Physics and Astronomy, Rutgers University, Piscataway, New Jersey*

²*Department of Physics, National Taiwan University, Taipei 10617, Taiwan 08855,*
USA

³*National Institute for Materials Science, 1-1 Namiki, Tsukuba, 305-0044,*
Japan

One of the enduring challenges in graphene research and applications is the extreme sensitivity of its charge carriers to external perturbations, especially those introduced by the substrate. The best available substrates to date, graphite and hBN, still pose limitations: graphite being metallic does not allow gating, while both hBN and graphite having lattice structures closely matched to that of graphene, may cause significant band structure reconstruction. Here we show that the atomically smooth surface of exfoliated MoS₂ provides access to the intrinsic electronic structure of graphene without these drawbacks. Using scanning tunneling microscopy and Landau-level spectroscopy in a device configuration which allows tuning the carrier concentration, we find that graphene on MoS₂ is ultra-flat producing long mean free paths, while avoiding band structure reconstruction. Importantly, the screening of the MoS₂ substrate can be tuned by changing the position of the Fermi energy with relatively low gate voltages. We show that shifting the Fermi energy from the gap to the edge of the conduction band gives rise to enhanced screening and to a substantial increase in the mean-free-path and quasiparticle lifetime. MoS₂ substrates thus provide unique opportunities to access the intrinsic electronic properties of graphene and to study *in situ* the effects of screening on electron-electron interactions and transport.

The vulnerability of atomically thin layers such as graphene^{1,2,3,4} to environmental disturbances has prompted an ongoing search for substrates that can support the material without perturbing its electronic structure. Graphite substrates were found to be by far the least invasive, making it possible to observe the intrinsic low energy spectrum of graphene by using scanning tunneling microscopy (STM), spectroscopy (STS)^{4,5} and cyclotron resonance (CR)⁶ measurements. However the metallic screening of graphite, which precludes control of the carrier-density by gating imposes severe limitations for both applications and fundamental studies. The alternative is to use insulating substrates, but the versatility gained comes at the price of enhanced sensitivity to surface corrugations,⁷ and impurities,⁸ which create electron-hole puddles that obscure the low energy electronic properties.⁹ These perturbations can be mitigated by the use of atomically flat substrates such as mica¹⁰ or hexagonal boron-nitride (hBN).^{11,12} However a close match between the lattice structure of graphene and the substrate, as is the case of hBN or graphite, leads to a spatial modulation observed as a Moiré pattern in topography which can significantly perturb the electronic spectrum.^{13,14,15} Here we show that atomically flat MoS₂ substrates provide access to the intrinsic band structure of graphene while at the same time they allow tuning via a gate voltage both the carrier density and the strength of screening.

MoS₂ is a semiconductor in the layered transition-metal-dichalcogenite family consisting of covalently bonded S-Mo-S sheets held together by the van der Waals force. Its weak interlayer coupling facilitates the extraction of ultra-thin layers by exfoliation. Bulk MoS₂ has an indirect band gap of 1.2 ~ 1.3 eV,¹⁶ which due to quantum confinement, crosses over to a direct band gap of ~1.9 eV when the material is exfoliated down to a monolayer.¹⁷ Thin layers of MoS₂ are well suited to serve as the channel material in field-effect transistor applications, exhibiting high mobility, almost ideal switching characteristics, and low standby power dissipation.^{18,19, 20, 21,22} The fact

that the position of E_F can be promoted from the gap to the conduction band (CB) with modest gate voltages, allows tuning the screening properties of MoS₂ films from insulating to metallic. Further, the absence of dangling bonds and of surface states renders its surface inert, clean and minimally invasive.²³ The large lattice mismatch between MoS₂ and graphene, together with its chemical inertness and the tunable screening, renders MoS₂ ideally suited for gated STM/STS studies of graphene.²⁴

We employed MoS₂ flakes exfoliated from bulk 2H-MoS₂ crystals and deposited onto a 300 nm chlorinated SiO₂ substrate capping a degenerately p-doped Si gate. The thickness of the MoS₂ flakes, as measured by atomic force microscopy (AFM), ranged from monolayer to 40 nm. Exfoliated graphene was subsequently deposited on the MoS₂ flakes.¹¹ The devices were measured in a home-built STM.^{25,26} Topography images were acquired in constant current mode. Differential conductance, dI/dV , which is proportional to the local density of states (LDOS),²⁷ was measured with a lock-in technique with fixed tip to sample distance. For details on sample fabrication and measurements see Supplemental Material S1.²⁸

Figure 1(a) illustrates the measurement setup and electrode configuration. The STM topography of graphene on MoS₂, Figure 1(b), is compared to that on chlorinated SiO₂, Figure 1(c), and on two hBN substrates with and without moiré pattern, in Figure 1(e) right and left panels respectively. In Figure 1(d,f) we show the height histograms obtained from these topography images. The average surface corrugation, calculated from the standard deviation of Gaussian fits to the height histograms, is 27 ± 0.2 pm and 31 ± 0.1 pm on the MoS₂ on hBN substrates respectively. This is significantly smaller than the corrugation on SiO₂, $\sim 234 \pm 0.8$ pm, in agreement with earlier reports.^{7,29} We note that the presence of the moiré pattern (Figure 1(e) right panel) leads to a substantially larger corrugation for graphene on hBN. In this case, in spite of the atomically flat hBN, the image exhibits a large periodic corrugation with an

apparent height of $\sim 0.4 \text{ nm}$ ³⁰ (Supplemental Material S2,²⁸). The difference between the two images in Figure 1(e), both showing the topography of graphene on hBN, is due to the relative twist angle, ϕ , between the lattice orientations of sample and substrate. The twist angle plays an important role at small lattice mismatch, $\delta = |a - a_s| / a_s$, as is the case for graphene on graphite,¹³ $\delta \sim 0$, and on hBN,²⁹ $\delta \sim 1.8\%$. Here a_s and a are the lattice constants of the substrate and graphene respectively. At small δ a moiré superstructure forms with an angle dependent super-period,²⁹

$$\lambda = a \frac{(1 + \delta)}{\sqrt{2(1 + \delta)(1 - \cos \phi) + \delta^2}}, \text{ which can open gaps}^{33,15} \text{ or introduce Van-Hove}$$

singularities¹³ at energies corresponding to the superstructure reciprocal vector. Thus, depending on ϕ , substrates with small δ can significantly disturb both the topography and the band structure even when they are atomically flat: the smaller ϕ , the lower the energy at which band reconstruction sets in. In contrast, no reconstruction is expected for substrates with large δ , as in the case of graphene on MoS₂ where $\delta \sim 0.3$.³¹ As a result there is no need for special precautions about substrate orientation when depositing graphene on MoS₂.

Figure 2 shows the gate voltage (V_g) dependence of the STS spectra and of the Dirac point energy (E_D) measured with respect to E_F , which is taken as the zero of energy. To understand the results for graphene on MoS₂ we first consider the case of graphene deposited on a chlorinated SiO₂ substrate, shown in Figure 2(b). In this case the data follow the typical square root dependence, $E_D = \hbar v_F \sqrt{\pi \alpha |V_g - V_0|}$, expected for the massless Dirac fermion spectrum of isolated graphene.^{2,4} Here \hbar is the reduced Planck constant and $v_F = 1.1 \pm 0.02 \times 10^6 \text{ m/s}$ is the Fermi velocity obtained, as discussed below, from the LL spectra. Fitting the data for these parameters we obtain the offset, $V_0 \sim 12 \text{ V}$, and the reduced gate capacitance $\alpha \approx 7.3 \times 10^{10} \text{ cm}^{-2} \text{V}^{-1}$, from

which we estimate the unintentional hole concentration, $n_0 = \alpha V_0 \sim 9 \times 10^{11} \text{ cm}^{-2}$. This value falls within the accepted range for graphene on SiO₂.² Expressing the reduced gate capacitance, $\alpha = \frac{\epsilon \epsilon_0}{de}$, in terms of the substrate thickness, $d = 300 \text{ nm}$, and the dielectric constant, ϵ , we obtain $\epsilon_{\text{SiO}_2} \sim 4.1$ consistent with the accepted value for the dielectric constant of SiO₂. Here e is the fundamental unit of charge and ϵ_0 the permittivity of free space.

Turning to graphene on MoS₂, Figure 2(c), we find that for $V_g < -10 \text{ V}$ the data are consistent with the expected square root dependence (solid line) calculated for the parameters obtained from the LL spectra: $v_F = 1.21 \pm 0.02 \times 10^6 \text{ m/s}$, $\alpha \approx 6.6 \times 10^{10} \text{ cm}^{-2}\text{V}^{-1}$, and $V_0 \sim -4.5 \text{ V}$. This gives an unintentional initial electron concentration of $n_0 = 7 \times 10^{11} \text{ cm}^{-2}$ and, using the thickness of the MoS₂ layer $d \sim 30 \text{ nm}$, we obtain $\epsilon_{\text{MoS}_2} \sim 3.7$ for the dielectric constant of MoS₂. In contrast, for $V_g > -10 \text{ V}$ the gate dependence is significantly weaker, indicating that most of the gate induced charge is taken up by the MoS₂ substrate. Indeed from the finite field data, presented below, we find that in this regime only $\sim 25\%$ of the gate induced charge goes to the graphene layer, the rest being absorbed by the MoS₂ substrate.²¹ This suggests that E_F has entered the CB of MoS₂ at which point the gate induced shift in the position of E_D is determined by the LDOS of the combined graphene/MoS₂ system, as illustrated in the inset of Figure 2(c). Naturally, as the LDOS in the CB of MoS₂ is larger than that of graphene most of the charge is absorbed by the former.

In the presence of a magnetic field normal to the graphene layer the spectrum breaks up into a sequence of LLs. Their evolution with field for the MoS₂ and SiO₂ substrates is shown in Figures 3(a) and 3(b) respectively. In both cases the sequence follows the field and level index (N) dependence characteristic of massless Dirac fermions:^{4,32}

$$E_N = E_D \pm v_F \sqrt{2e\hbar|N|B} \quad N = 0, \pm 1, \pm 2 \dots \quad (1)$$

Here $N > 0$ ($N < 0$) and $+$ ($-$) correspond to electron (hole) levels. Fitting the measured sequence to this expression we obtain $v_F(\text{SiO}_2) = 1.1 \pm 0.02 \times 10^6$ m/s on chlorinated SiO₂ consistent with reported values.² In the case of graphene on MoS₂ where no prior measurements have been reported we find $v_F(\text{MoS}_2) = 1.21 \pm 0.02 \times 10^6$ m/s. This gives the ratio $v_F(\text{MoS}_2) / v_F(\text{SiO}_2) \sim 1.1$ which is comparable to the ratio of the dielectric constants, $\epsilon_{\text{SiO}_2} / \epsilon_{\text{MoS}_2} \sim 1.1$, consistent with the expected inverse dependence of v_F on the dielectric constant.³³

One of the prerequisites for observing well developed LLs is for the random potential to be smooth on the length scale of the cyclotron orbit, $l_c(B) = \sqrt{\frac{\hbar}{eB}} = \frac{25.64 \text{ nm}}{\sqrt{B}}$. The field at which LLs become resolved signals that the cyclotron orbit is sufficiently small to “fit” within the characteristic puddle size of a particular sample³⁴ and provides a direct measure of the quasiparticle mean free path (mfp) and sample quality. For graphene on MoS₂, Figure 3(a), the LLs are already resolved at 2 T indicating a characteristic puddle size exceeding $l_c(2 \text{ T}) \sim 18$ nm. In contrast for the SiO₂ substrate, Figure 3(a), LLs only become distinguishable at 6 T, indicating smaller puddles, bounded by $l_c(6 \text{ T}) \sim 10$ nm, and hence a shorter mfp. To test this conclusion we directly imaged the electron-hole puddles by mapping the spatial dependence of the doping level. For the SiO₂ substrate, Figures 3(c), the average puddle size obtained from the map, ~ 10 nm, is consistent with that obtained from the LL onset field. For the MoS₂ substrate, Figures 3(d), the larger puddle size obtained from the maps, ~ 30 nm, suggests that the LL would remain well resolved down to magnetic fields of 0.5 T, which are below the measurement range reported here. This value is slightly larger than for graphene on hBN³⁵, providing yet another indication of the high quality of the MoS₂ substrates.

To study the effect of doping on the LLs we measured the gate dependence of the spectra at fixed field, Figure 4(a) (10 T data shown in Supplemental Material S4,²⁸). The pronounced staircase features reflect the high degeneracy of the LLs each of which can accommodate a carrier density of $D = 4 \frac{B}{\phi_0} = 10^{11} \text{ B[T] states/cm}^2$, where $\phi_0 = 4.14 \times 10^{-11} \text{ Tcm}^2$, is the fundamental unit of flux.⁴ In the process of gating, each LL as it is being filled pins the Fermi energy, and this produces the plateau features.³⁶ Since the width of a plateau, $\Delta V_g = D / \alpha$, reflects the gate voltage required to fill one LL, it provides a direct measure of α . In the regime where the MoS₂ substrate is insulating, $V_g < -10 \text{ V}$, we find $\Delta V_g = 11.8 \text{ V}$, which gives $\alpha \approx 6.6 \times 10^{10} \text{ cm}^{-2} \text{V}^{-1}$. For $V_g > -10 \text{ V}$, the plateaus become much wider, $\Delta V_g \sim 50 \text{ V}$ and $\alpha \approx 1.5 \times 10^{10} \text{ cm}^{-2} \text{V}^{-1}$, indicating the entry of E_F into the CB of MoS₂. At this point $\sim 75\%$ of the carriers introduced by the gate are taken up by the MoS₂ substrate which can now provide better screening of the random potential.

In Figure 4(b) we present the LL spectra for several values of V_g . Extracting ν_F , Figure 4(c), we find that it is independent of V_g . Since ν_F is inversely proportional to ϵ this implies that, in spite of the increased screening accompanying the entry of E_F into the CB, the dielectric constant of MoS₂ is independent of doping for the range of V_g employed here, consistent with recent theoretical work.³⁷

To illustrate the effect of screening on the quasiparticle lifetime we compare in Figure 4(d) the linewidth, ΔE , of the $N = 0$ LL in the unscreened ($V_g = -30 \text{ V}$) and screened regimes ($V_g = +25 \text{ V}$). Using a Gaussian fit we find $\Delta E \sim 53.5 \text{ mV}$ for the unscreened case, which corresponds to a lifetime of $\tau \approx \hbar / \Delta E = 12 \text{ fs}$ and to a mfp of $l_{mfp} \sim \nu_F \tau \sim 15 \text{ nm}$. In the screened regime we find a much narrower linewidth, $\Delta E \sim 28.2 \text{ mV}$, indicating significant reduction in scattering with correspondingly longer lifetimes $\sim 23 \text{ fs}$ and a mfp of $l_{mfp} \sim 28 \text{ nm}$. Interestingly the mfp obtained from the N

$= 0$ LL linewidth is comparable to the average puddle size, in Figure 3(c), indicating that for these samples the electron-hole puddles are the main source of scattering. A similar analysis of the $N = 0$ LL on chlorinated SiO_2 (Figure 3b) gives $\tau \sim 10$ fs and $l_{mfp} \sim 11$ nm comparable to the puddle sizes in this system, so that here also electron-hole puddles are the main source of scattering.

In summary, the quality of MoS_2 substrates as measured by the mfp is remarkably good: in the unscreened regime it is comparable to that in the best insulating substrates, hBN and chlorinated SiO_2 , while in the screened regime it is larger still. The results presented here demonstrate that MoS_2 substrates are well suited for accessing the low energy electronic properties of graphene while at the same time providing great flexibility through controllable carrier densities and tunable screening.

Funding was provided by DOE-FG02-99ER45742 (E.Y.A, G.L), NSF DMR 1207108 (C.P.L) and National Science Council of Taiwan (C.P.L). We thank Ivan Skachko and Jinhai Mao for useful discussions.

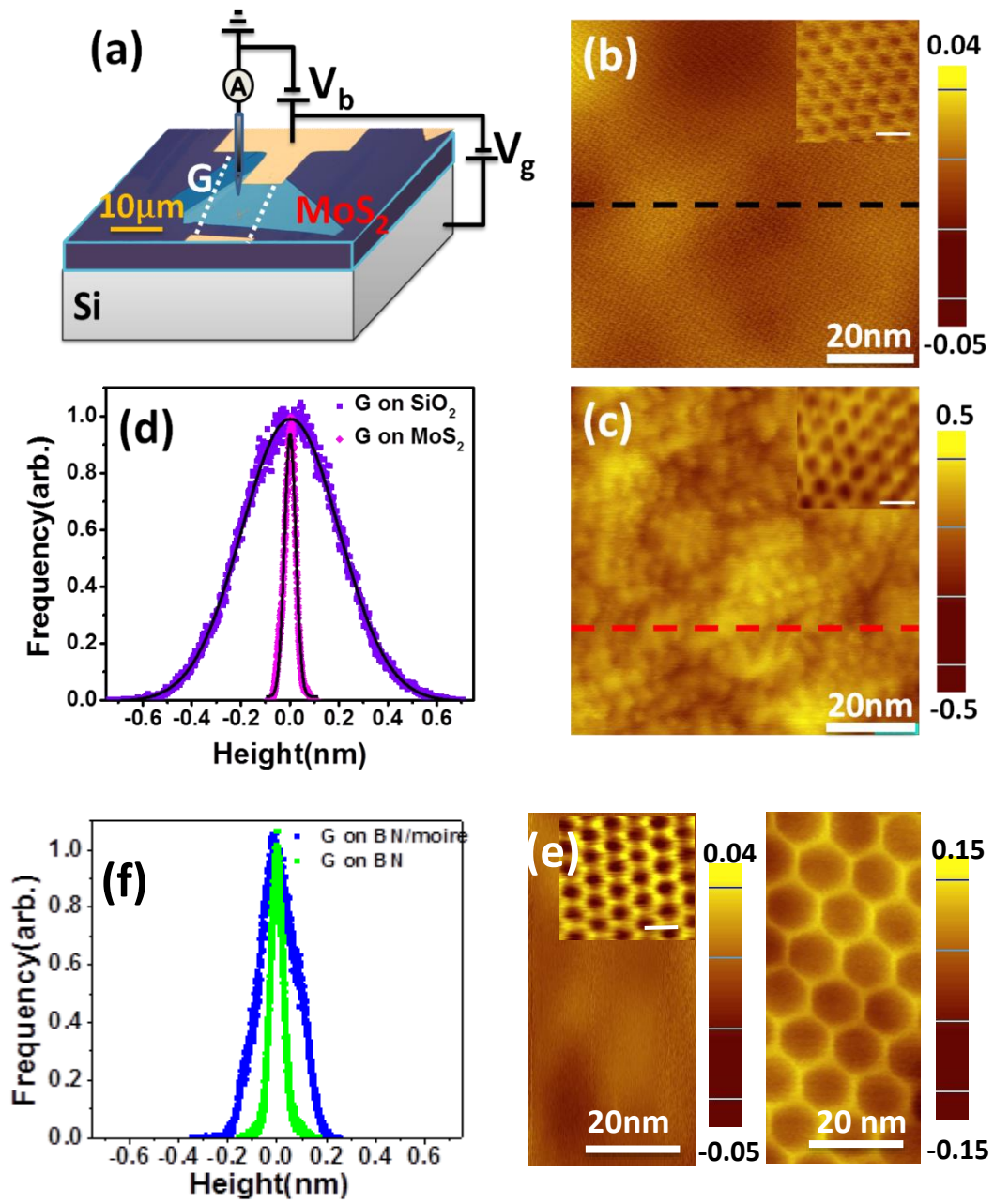


Figure 1. (a) Schematic of STS measurement setup showing the graphene sample (G) and MoS₂ substrate. The sample bias V_b is applied between the STM tip and the sample. The edge of the graphene flake is marked by dashed lines. The back gate voltage V_g is applied between the Si substrate and the top electrode. (b), (c) STM topography of graphene on MoS₂ and on chlorinated SiO₂ respectively. (d) Height histograms of the topography images in b and c. (e) Same as (b) for graphene on hBN with (right) and without (left) moiré pattern. (f) Height histograms of the topography images in (e). Image area 80 nm × 80 nm (b,c) and 40 nm × 80 nm (e). Insets in (b,c,e) represent zoom-in images with scale bar 0.3 nm. STS parameters: set point current $I = 20$ pA at $V_b = 0.4$ V. Height profiles shown in Supplemental material SM2 are taken along the dashed lines in (b),(c).

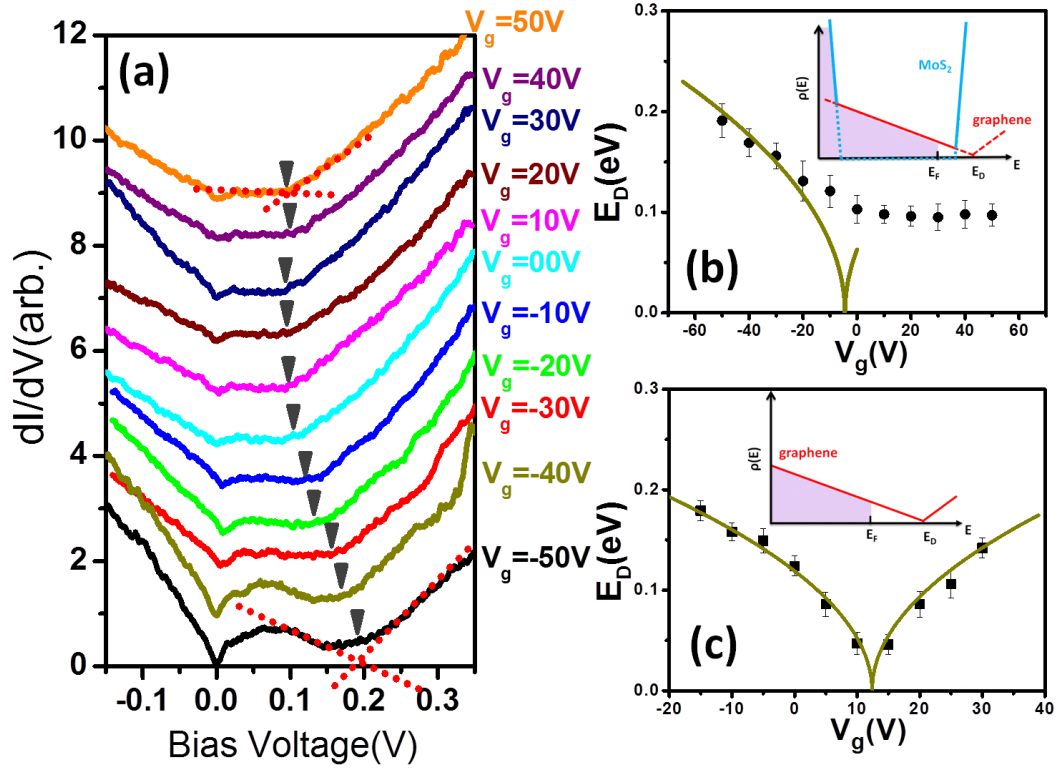


Figure 2. (a) Gate-voltage dependence of dI/dV spectra for graphene MoS₂. Arrows indicate the position of the Dirac point, E_D . Curves are vertically displaced for clarity. (b) Gate-voltage dependence of E_D for graphene on a thin (~30 nm) MoS₂ substrate. The solid line represents a fit to the data as described in the text. Inset: Sketch of the combined DOS (solid lines) of graphene (dashed red lines) and MoS₂ substrate (dashed teal lines). (c) Same as (b) for graphene on a chlorinated SiO₂ substrate. Inset: Sketch of the DOS of p-doped graphene on an insulating substrate for energies within the substrate gap. STS parameters: set point current $I = 20$ pA at $V_b = 0.35$ V, modulation amplitude $5mV_{\text{rms}}$.

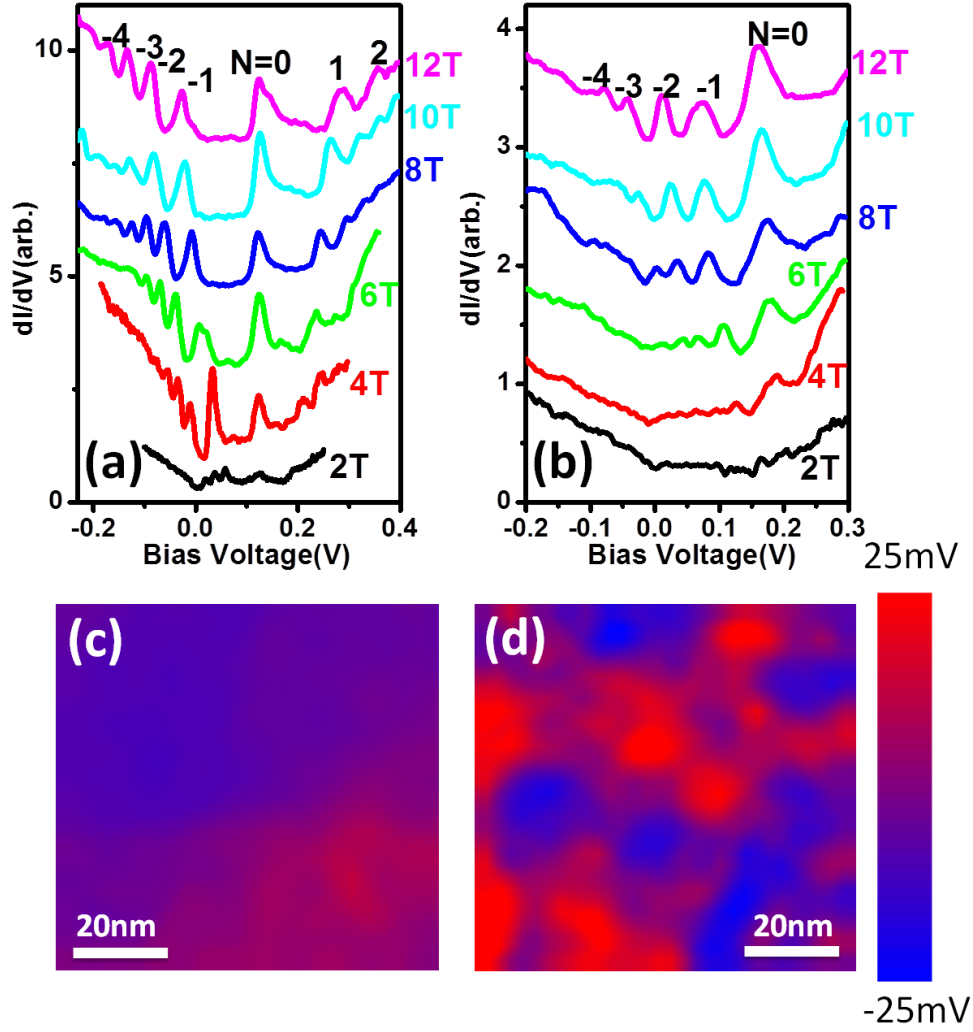


Figure 3. Field dependence of LL spectra. (a),(b) Spectra for graphene on MoS_2 and on SiO_2 , respectively at $V_g = 10$ V. The LL indices $N = 0, \pm 1, \pm 2, \dots$ are marked. (c),(d) Spatial variation of the $N = -1$ peak position at $B = 10$ T obtained from a dI/dV map at $V_g = 0$ V representing the doping inhomogeneity in graphene: blue (red) corresponds to hole (electron) doping. STS parameters: set-point $I = 20$ pA, $V_b = 0.35$ V, modulation amplitude 2mV_{rms}

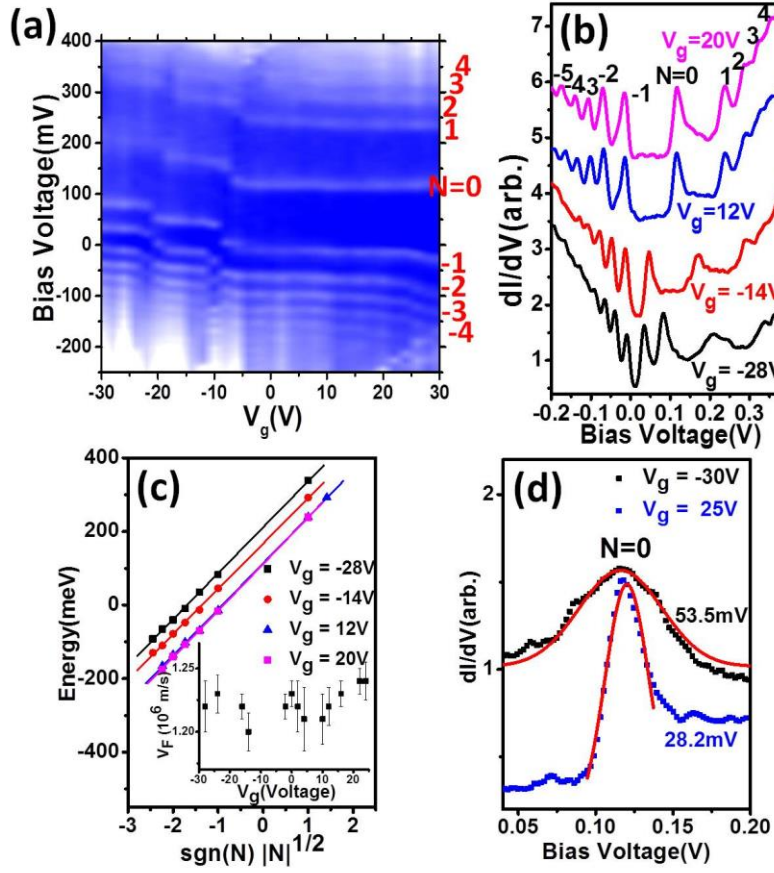


Figure 4. (a) Intensity map representing the gate dependence of the dI/dV spectra of graphene on MoS₂ at 8 T. Each vertical line corresponds to a LL spectrum at a particular gate-voltage. White staircase pattern corresponds to the LL peaks as indicated by the level-index N . STS parameters: set point current $I = 20$ pA, $V_b = 0.4$ V, ac modulation 5 mV_{rms}. (b) Gate-voltage dependence of LL spectra. (c) Gate-voltage dependence of LL peak sequences. Solid symbols are data points and lines are fits to equation 1. Inset: Gate dependence of Fermi velocity. (d) Comparison of the linewidth for the $N = 0$ LL in the unscreened ($V_g = -30$ V) and screened ($V_g = 25$ V) regimes. Symbols and lines represent data points and Gaussian fits respectively. Curves are offset for clarity.

References:

- ¹ K. S. Novoselov, A. K. Geim, S. V. Morozov, D. Jiang, Y. Zhang, S. V. Dubonos, I. V. Grigorieva, and A. A. Firsov, *Science* **306** (5696), 666 (2004).
- ² A. H. Castro Neto, F. Guinea, N. M. R. Peres, K. S. Novoselov, and A. K. Geim, *Reviews of Modern Physics* **81** (1), 109 (2009).
- ³ D. S. L. Abergel, V. Apalkov, J. Berashevich, K. Ziegler, and Tapash Chakraborty, *Advances in Physics* **59** (4), 261 (2010).
- ⁴ E. Y. Andrei, G. Li, and X. Du, *Reports on Progress in Physics* **75** 056501 (2012).
- ⁵ G. Li, A. Luican, and E. Y. Andrei, *Physical Review Letters* **102** (17), 176804 (2009).
- ⁶ P. Neugebauer, M. Orlita, C. Faugeras, A. L. Barra, and M. Potemski, *Physical Review Letters* **103** (13), 136403 (2009).
- ⁷ Masa Ishigami, J. H. Chen, W. G. Cullen, M. S. Fuhrer, and E. D. Williams, *Nano Letters* **7** (6), 1643 (2007).
- ⁸ E. H. Hwang, S. Adam, and S. Das Sarma, *Physical Review Letters* **98** (18), 186806 (2007).
- ⁹ J. Martin, N. Akerman, G. Ulbricht, T. Lohmann, J. H. Smet, K. Von Klitzing, and A. Yacoby, *Nat. Phys.* **4** (2), 144 (2008).
- ¹⁰ C. H. Lui, L. Liu, K. F. Mak, G. W. Flynn, and T. F. Heinz, *Nature* **462** (7271), 339 (2009).
- ¹¹ C. R. Dean, A. F. Young, MericI, LeeC, WangL, SorgenfreiS, WatanabeK, TaniguchiT, KimP, K. L. Shepard, and HoneJ, *Nature nanotechnology* **5** (10), 722 (2010).
- ¹² S. M. Kim, A. Hsu, P. T. Araujo, Y. H. Lee, T. Palacios, M. Dresselhaus, J. C. Idrobo, K. K. Kim, and J. Kong, *Nano Letters* **13** (3), 933 (2013).
- ¹³ G. Li, A. Luican, J. M. B. L. dos Santos, A. H. C. Neto, A. Reina, J. Kong, and E. Y. Andrei, *Nat. Phys.* **6** (2), 109 (2010).
- ¹⁴ G. Giovannetti, P. A. Khomyakov, G. Brocks, P. J. Kelly, and J. van den Brink, *Physical Review B* **76** (7), 073103 (2007).
- ¹⁵ C. R. Woods, L. Britnell, A. Eckmann, R. S. Ma, J. C. Lu, H. M. Guo, X. Lin, G. L. Yu, Y. Cao, R. V. Gorbachev, A. V. Kretinin, J. Park, L. A. Ponomarenko, M. I. Katsnelson, Yu N. Gornostyrev, K. Watanabe, T. Taniguchi, C. Casiraghi, H. J. Gao, A. K. Geim, and K. S. Novoselov, *Nat Phys* **10** (6), 451 (2014).
- ¹⁶ K. K. Kam and B. A. Parkinson, *J Phys Chem-Us* **86** (4), 463 (1982).

- 17 A. Splendiani, L. Sun, Y. B. Zhang, T. S. Li, J. Kim, C. Y. Chim, G. Galli,
and F. Wang, *Nano Letters* **10** (4), 1271 (2010).
- 18 B. Radisavljevic, A. Radenovic, J. Brivio, V. Giacometti, and A. Kis, *Nature*
nanotechnology **6** (3), 147 (2011).
- 19 H. Wang, L. L. Yu, Y. H. Lee, Y. M. Shi, A. Hsu, M. L. Chin, L. J. Li, M.
Dubey, J. Kong, and T. Palacios, *Nano Letters* **12** (9), 4674 (2012).
- 20 Z. Y. Yin, H. Li, H. Li, L. Jiang, Y. M. Shi, Y. H. Sun, G. Lu, Q. Zhang, X. D.
Chen, and H. Zhang, *ACS Nano* **6** (1), 74 (2012).
- 21 K. Roy, M. Padmanabhan, S. Goswami, T. P. Sai, G. Ramalingam, S.
Raghavan, and A. Ghosh, *Nature nanotechnology* **8** (11), 826 (2013).
- 22 W. Zhang, C. P. Chuu, J. K. Huang, C. H. Chen, M. L. Tsai, Y. H. Chang, C.
T. Liang, Y. Z. Chen, Y. L. Chueh, J. H. He, M. Y. Chou, and L. J. Li,
Scientific reports **4**, 3826 (2014).
- 23 A. V. Kretinin, Y. Cao, J. S. Tu, G. L. Yu, R. Jalil, K. S. Novoselov, S. J.
Haigh, A. Gholinia, A. Mishchenko, M. Lozada, T. Georgiou, C. R. Woods, F.
Withers, P. Blake, G. Eda, A. Wirsig, C. Hucho, K. Watanabe, T. Taniguchi,
A. K. Geim, and R. V. Gorbachev, *Nano Letters* **14** (6), 3270 (2014).
- 24 Chih-Pin Lu, Guohong Li, Jinhai Mao, Li-Min Wang, and Eva Y. Andrei,
Nano Letters **14** (8), 4628 (2014).
- 25 G. Li and E. Y. Andrei, *Nature Physics* **3** (9), 623 (2007).
- 26 G. Li, A. Luican, and E. Y. Andrei, *The Review of scientific instruments* **82**
(7), 073701 (2011).
- 27 J. Tersoff and D. R. Hamann, *Physical Review B* **31** (2), 805 (1985).
- 28 See supplementary material.
- 29 J. M. Xue, J. Sanchez-Yamagishi, D. Bulmash, P. Jacquod, A. Deshpande, K.
Watanabe, T. Taniguchi, P. Jarillo-Herrero, and B. J. Leroy, *Nat Mater* **10**
(4), 282 (2011).
- 30 P. Xu M. Neek-Amal, D. Qi, P. M. Thibado, L. O. Nyakiti, V. D. Wheeler, R.
L. Myers-Ward, C. R. Eddy Jr., D. K. Gaskill, F.M. Peeters,
arXiv:1407.1189v1 (2014).
- 31 Yumeng Shi, Wu Zhou, Ang-Yu Lu, Wenjing Fang, Yi-Hsien Lee, Allen
Long Hsu, Soo Min Kim, Ki Kang Kim, Hui Ying Yang, Lain-Jong Li, Juan-
Carlos Idrobo, and Jing Kong, *Nano Letters* **12** (6), 2784 (2012);
Yandong Ma, Ying Dai, Meng Guo, Chengwang Niu, and Baibiao Huang,
Nanoscale **3** (9), 3883 (2011).
- 32 M. O. Goerbig, *Reviews of Modern Physics* **83** (4), 1193 (2011).
- 33 C. Hwang, D. A. Siegel, S. K. Mo, W. Regan, A. Ismach, Y. G. Zhang, A.
Zettl, and A. Lanzara, *Scientific reports* **2**, 590 (2012).

- ³⁴ A. Luican, G. Li, and E.Y. Andrei, *Phys. Rev. B* **83**, 041405(R) (2011).
- ³⁵ J. S. Chae, S. Jung, A. F. Young, C. R. Dean, L. Wang, Y. D. Gao, K. Watanabe, T. Taniguchi, J. Hone, K. L. Shepard, P. Kim, N. B. Zhitenev, and J. A. Stroscio, *Physical Review Letters* **109** (11), 116802 (2012).
- ³⁶ Adina Luican-Mayer, Maxim Kharitonov, Guohong Li, Chih-Pin Lu, Ivan Skachko, Alem-Mar B. Gonçalves, K. Watanabe, T. Taniguchi, and Eva Y. Andrei, *Physical Review Letters* **112** (3), 036804 (2014).
- ³⁷ E. J. G. Santos and E. Kaxiras, *ACS Nano* **7** (12), 10741 (2013).